Anticancer potential of NSAID-derived tris(pyrazolyl)methane ligands in iron(ii) sandwich complexes

Anticancer Potential of NSAID-derived Tris(pyrazolyl)methane Ligands in Iron(II) Sandwich Complexes

Alberto Gobbo,[a] Sarah A.P. Pereira,[b,c] Fátima A.R. Mota,[b] Irina Sinenko,[c] Kseniya Glinkina,[c] Dario Rocchi,[a] Massimo Guelfi,[a] Tarita Biver,[a] Chiara Donati,[d] Stefano Zacchini,[e] M. Lúcia M. F. S. Saraiva,[b] Paul J. Dyson,[c] Fabio Marchetti [a,*]

[a] University of Pisa, Department of Chemistry and Industrial Chemistry, Via G. Moruzzi 13, I-56124 Pisa, Italy.

[b] LAQV, REQUIMTE, Laboratório de Química Aplicada, Faculdade de Farmácia da Universidade do Porto, Portugal.

[c] Institut des Sciences et Ingénierie Chimiques, Ecole Polytechnique Fédérale de Lausanne (EPFL), CH 1015, Switzerland.

[d] University of Padova, Department of Pharmaceutical and Pharmacological Sciences, Via F. Marzolo 5, I-35131 Padova, Italy.

[e] University of Bologna, Department of Industrial Chemistry "Toso Montanari", Via P. Gobetti 85, I-40129 Bologna, Italy

Corresponding Author

*E-mail address: fabio.marchetti@unipi.it

Webpage: https://people.unipi.it/fabio_marchetti/

Abstract

Tris(pyrazolyl)methane (**tpm**), 2,2,2-tris(pyrazolyl)ethanol (**tpm^{OH}**) and its esterification derivatives with ibuprofen and flurbiprofen (**tpm^{IBU}** and **tpm^{FLU}**) were used as ligands to obtain complexes of the type [Fe(tpm^{X})$_2$]Cl$_2$ (**1-4**). The **tpm^{IBU}** and **tpm^{FLU}** ligands and corresponding complexes **3** and **4** were characterized by IR and multinuclear NMR spectroscopy, and the structure of **tpm^{IBU}** was elucidated by single crystal X-ray diffraction. Complexes **1-4** were also assessed for their behaviour in aqueous media (solubility in D_2O, octanol/water partition coefficient, stability in physiological-like conditions). The antiproliferative activity of ligands and complexes was determined on A2780, A2780cis and A549 cancer cell lines and the non-cancerous HEK 293T and BJ cell lines. The ligands and complexes were investigated for their ability to inhibit COX-2 (cyclooxygenase) and HNE (4-hydroxynonenal) enzymes. Complexes **3** and **4** exhibited cytotoxicity that may be attributed predominantly to their bioactive fragments, while DNA binding and enhancement of ROS production do not appear to play any significant role.

Keywords: Anticancer metal complexes; bioinorganic chemistry; iron(II) complexes; tris(pyrazol-1-yl)methane; cytotoxicity; NSAIDs.

1. Introduction

Transition metal complexes exhibit unique properties with important medicinal applications.[1,2,3,4] A few platinum-based drugs are currently used worldwide for treating several types of cancers,[5,6,7] but they have limitations, such as progressively acquired resistance during the treatment and collateral effects essentially associated with toxicity.[8,9,10] To address these challenges, many transition metal complexes have been evaluated as possible alternatives.[11,12,13,14] Among these, iron compounds have been intensively investigated, with organo-iron complexes emerging as promising candidates.[15,16,17,18] Ferrocene ($FeCp_2$, Cp = η^5-C_5H_5) represents the simplest member of this category, and while it is inactive as an anticancer agent, the introduction of suitable substituents on the cyclopentadienyl rings

can confer significant cytotoxicity to the resulting complexes.[19,20] Generally, one of the modes of action for these complexes involves Fe^{II} to Fe^{III} oxidation in tumour cells, disrupting cellular redox homeostasis by increasing the production of reactive oxygen species (ROS).[21] However, certain ferrocene derivatives are highly hydrophobic, which potentially limits their possible pharmacological application due to insufficient water solubility, a pre-requisite for drug development.[22] Furthermore, while a high Log P_{ow} value may enhance the cytotoxic activity by facilitating passive diffusion through the cell membrane,[23,24] it may otherwise trigger drug-induced adverse toxicity, a major cause of drug failure in clinical trials.[25] Note that Log P_{ow} values higher than 3 have been considered critical.[26]

Tris(pyrazolyl)methane (**tpm**) is a neutral compound (Figure 1) belonging to the family of scorpionates, acting as a robust, six-electron donor ligand when bound to a metal centre in a tridentate (κ^3) fashion.[27,28,29,30] The tpm core offers opportunities for functionalization, including the introduction of alkyl or aryl substituents on the pyrazolyl rings,[31,32,33] or by exploiting the slightly acidic character of the apical methylidyne {CH} group,[34] which leads to the so called "third generation scorpionates".[35,36,37] Specifically, deprotonation can be performed using a strong base, with the resulting carbanion being highly nucleophilic.[38]

The "tpm analogue" of ferrocene, i.e. the sandwich compound $[Fe(\kappa^3\text{-}\mathbf{tpm})_2]^{2+}$, has been reported in combination with various counteranions, and has been investigated in homogenous catalysis.[39,40] The $[Fe(\kappa^3\text{-}\mathbf{tpm})_2]^{2+}$ dication is water soluble, a favourable pre-requisite for drug development (see above),[41] yet the biological applications of $[Fe(\kappa^3\text{-}\mathbf{tpm})_2]^{2+}$ and more generally iron-tpm species, remain unexplored. Recently we disclosed that a ruthenium(II)-tpm system exhibits a considerable stability in physiological-like solutions, and a series of related complexes display a promising anticancer properties.[42,43] Additionally, the anticancer potential of a few other ruthenium(II)-tpm complexes was investigated previously.[44]

In this work, we report a comprehensive synthetic and biological study to evaluate the potential of iron(II) tpm compounds as anticancer agents. In particular, we demonstrate that the tpm ligand can

be derivatized with bioactive fragments, tuning the lipophilicity and supplying bioactive functionality to the resulting complexes. It is noteworthy that conjugating transition metal structures with organic compounds with a documented biological activity is a widely explored strategy trying to optimize the anticancer performance.[45,4647,48,49,50] Ideally, the two components should act in a complementary way, playing different roles and/or directing to different targets.[51] Specifically, ibuprofen and flurbiprofen (Figure 1) belong to the family of nonsteroidal anti-inflammatory drugs (NSAIDs), that are able to inhibit cyclooxygenase enzymes (COX) and human neutrophil elastase (HNE).[52,53] The skeletons of these two carboxylic acids have been tethered to a diversity of metal complexes, providing in some cases a notable synergistic effect, resulting in an enhancement of the anticancer activity.[54,55,56,57] In particular, a high level of COX-2 expression is found in cancer cells, and several studies demonstrate that cyclooxygenase inhibitors could be of benefit against the development and growth of tumours. Notably, combinatorial treatments of either chemotherapy or radiotherapy with COX-2 inhibitors have shown promising results.[58,59]

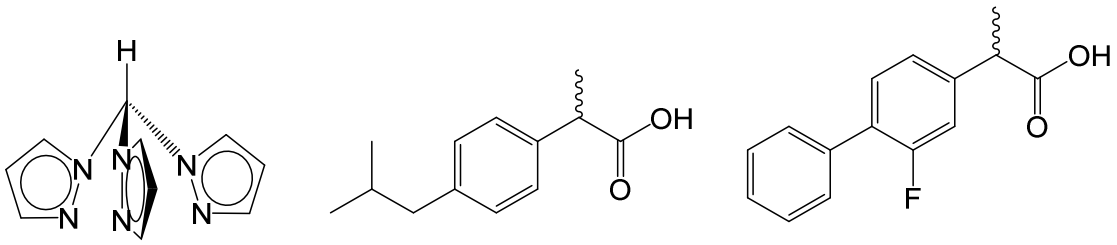

Figure 1. Structures of (from left to right): tris(pyrazolyl)methane (**tpm**), ibuprofen and flurbiprofen.

2. Results and discussion

2.1. Synthesis and structural characterization of ligands and complexes

$[Fe(\kappa^3\text{-}\mathbf{tpm})_2]^{2+}$ was prepared as its dichloride salt, $[Fe(\kappa^3\text{-}\mathbf{tpm})_2]Cl_2$ (**1**), in 60% yield using a modified synthesis with respect to the published procedure (see Experimental for details).[60] Since characterization data of **1** is sparse in the literature, we report comprehensive IR (solid state) and ^1H and ^{13}C NMR (CD_3OD solution) spectroscopic characterization. The X-ray structure of the cation of **1** was previously determined in association with distinct anions, *i.e.* an iron(III) based anion,[61] NO_3^-, [62] and BF_4^-. [63] Here, we provide the crystallographic characterization of the

hexafluorophosphate salt $[Fe(\kappa^3\text{-}\mathbf{tpm})_2][PF_6]_2$, **1'** (see Figure S1 and Table S1 in the Supporting Information).

We considered that previously reported 2,2,2-tris(pyrazolyl)ethanol (**tpm^{OH}**) could represent a convenient entry into functionalization chemistry with bioactive carboxylic acids. Therefore, **tpm^{OH}** was prepared using a literature procedure (see Scheme 1 and Experimental).[35] In order to derivatize **tpm^{OH}** with ibuprofen and flurbiprofen, these two carboxylic acids were initially converted into the corresponding acyl chlorides. Then, acyl chlorides were reacted with **tpm^{OH}** in the presence of ethylenediamine as the base. The resulting products, **tpm^{IBU}** and **tpm^{FLU}**, were consequently purified by column chromatography over silica and isolated in 95% and 36% yield, respectively. Attempts to obtain **tpm^{IBU}** and **tpm^{FLU}** using the Steglich protocol (direct carboxylic acid esterification)[64] was less efficient.

The IR spectra of the bio-functionalized ligands display the diagnostic absorption related to the ester group at around 1750 cm^{-1}. In the ^1H NMR spectra, signals related to the pyrazolyl rings undergo a negligible shift ongoing from **tpm^{OH}** to **tpm^{IBU}** or **tpm^{FLU}**. Salient ^{13}C features concern the methylene bound to the apical carbon of the tpm backbone and the ester carbon, observed at ca. 67 and 172 ppm, respectively ($CDCl_3$ solutions). The structure of **tpm^{IBU}** was ascertained by a single crystal X-ray diffraction study (Figure 1). Bonding parameters substantially resemble those previously reported for **tpm^{OH}** [65] and other ibuprofen-derived esters,[43,50] respectively.

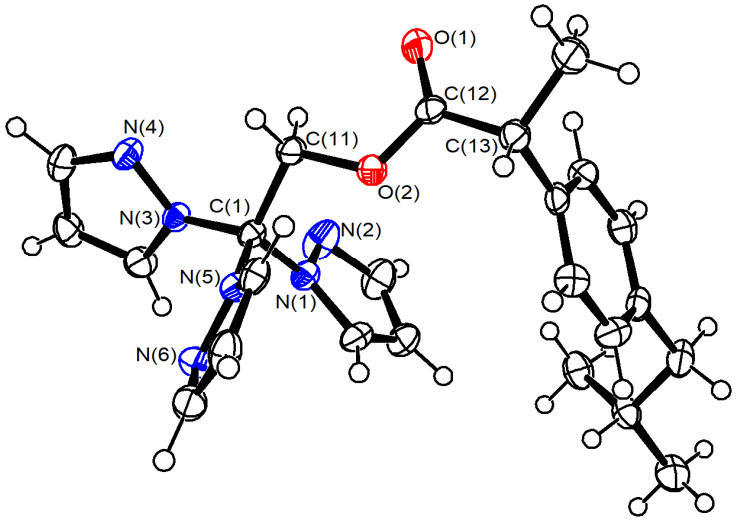

Figure 1. Molecular structure of **tpm^{IBU}**. Displacement ellipsoids are at the 50% probability level. Selected bond lengths (Å) and angles (°): C(1)-N(1) 1.4551(18), C(1)-N(3) 1.4517(18), C(1)-N(5) 1.4528(18), N(1)-N(2) 1.3584(18), N(3)-N(4) 1.3592(17), N(5)-N(6) 1.3564(17), C(1)-C(11) 1.527(2), C(11)-O(2) 1.4282(17), O(2)-C(12) 1.3457(18), C(12)-O(1) 1.1967(19), C(12)-C(13) 1.509(2), C(1)-C(11)-O(2) 106.09(11), C(11)-O(2)-C(12) 116.27(12), O(2)-C(12)-O(1) 122.55(14), O(2)-C(12)-C(13) 110.64(12), O(1)-C(12)-C(13) 126.81(14).

Complexes **3** and **4** were obtained by reacting iron dichloride hydrate with **tpm^{IBU}** or **tpm^{FLU}** in methanol at room temperature (Scheme 1)**,** and isolated as pink solids in 78% and 55% yield, respectively. The previously reported hydroxyl complex **2**, lacking the biomolecular fragments, was also prepared for comparison.[66] IR and NMR (^{1}H, ^{13}C and, in the case of **4**, ^{19}F) spectra of **3** and **4** do not show significant differences compared to **2** and **tpm^{IBU}** and **tpm^{FLU}**, respectively.

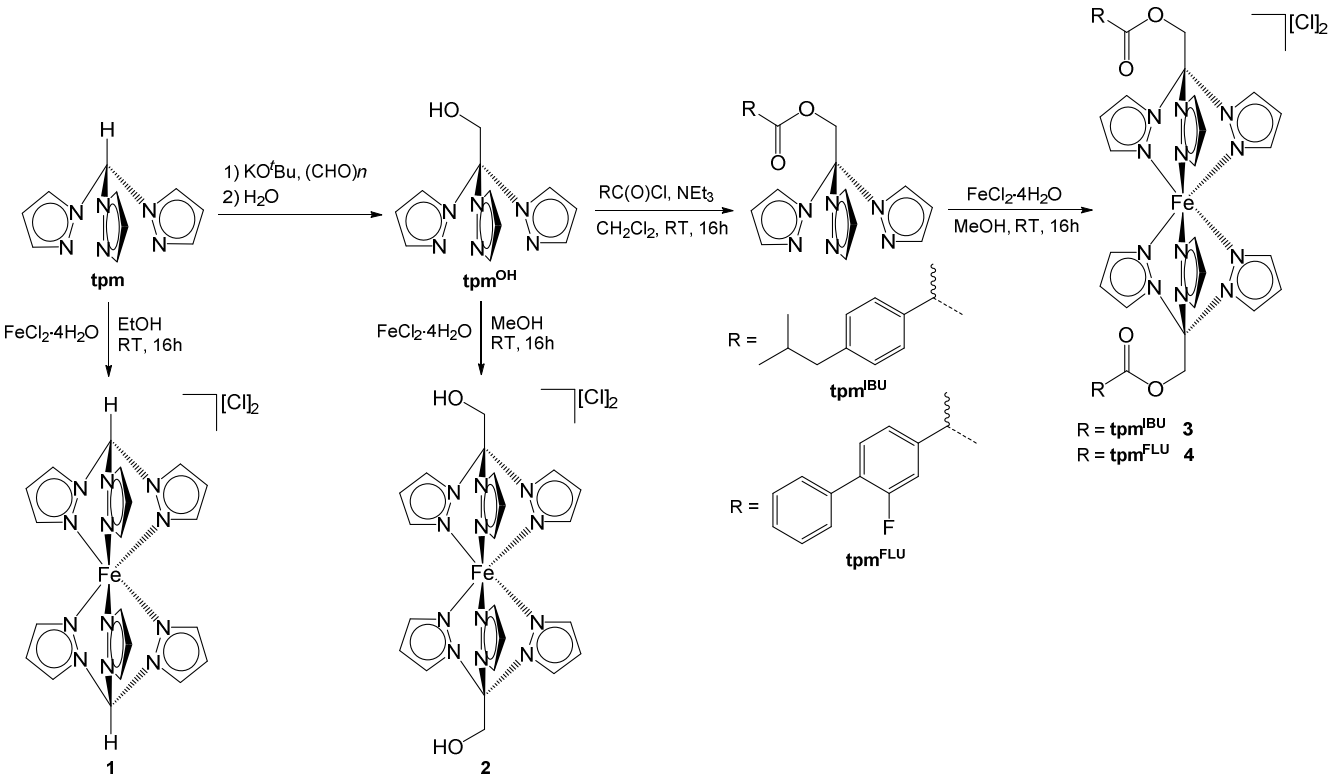

Scheme 1. Synthesis of bio-functionalized tris-pyrazolylmethane derivatives and corresponding iron(II) sandwich complexes.

2.2. Solubility, partition coefficients and stability in aqueous media

With a view to biological studies, we assessed the behaviour of **1-4** in aqueous media using established spectroscopic methods[42,67] (see Supporting Information for experimental details), and data are reported in Table 1. The solubility of **1** and **2** in D_2O at room temperature was determined by ^{1}H NMR spectroscopy employing dimethyl sulfone (Me_2SO_2) as an internal standard.[68] Complex

1 displays a high water solubility of 211 g/L (380 mM); for comparison, the estimated solubility of the reference drug cisplatin is 2.5 g/L (8.4 mM).[69] The solubility of **2** is also notable (28 mM), whereas the solubility values of **3** and **4** are below the threshold of the NMR method.

The octanol-water partition coefficients[70] of **2-4** were determined using UV-Vis spectroscopy,[71,72] outlining a substantial amphiphilicity ($-1 < \text{Log } P_{ow} < 1$), representing a compromise between lipophilicity and hydrophilicity (see Introduction). However, **3** and **4** are more lipophilic than **1** and **2**, as a consequence of the presence of an extensive hydrophobic fragment on each ligand, and in agreement with the solubility data.

The stability of **1-4** was monitored in aqueous solution by ^{1}H NMR spectroscopy at 37 °C over 48 hours. While **1** and **2** were analysed in neat D_2O and cell culture medium (DMEM), respectively, CD_3OD was used as a co-solvent for **3** and **4**, to reach an appreciable solubility. Complexes **1**, **3** and **4** exhibit good stability, and in particular **3** and **4** undergo negligible decomposition in the presence of the cell culture medium (≤ 5%). The ^{1}H NMR spectrum of **1** in DMEM contains low intensity signals that may be attributed to uncoordinated tris-pyrazolylmethane. Similarly, release of **tpm^{OH}** was detected for **2** in both solutions investigated, albeit to a higher extent, with only a moderate fraction of the starting material (27%) recovered in DMEM after 48 hours. Interestingly, when the solid residue obtained from the D_2O solution of **2** was recovered and dissolved in CD_3OD, the resulting ^{1}H NMR spectrum contained only signals of **2**, suggesting the reversibility of the **tpm^{OH}** dissociation process.

Table 1. Solubility in water (D_2O), octanol/water partition coefficients (Log P_{ow}) and residual iron complexes in aqueous solutions maintained at 37 °C for 48 h. [a] Calculated by ^{1}H NMR (Me_2SO_2 internal standard). [b] CD_3OD-D_2O (1:1 v/v) solution. [c] CD_3OD-DMEM-d (1:1 v/v) solution.

Complex	Solubility / mol·L^{-1} (D_2O, 21 °C) [a]	Log P_{ow}	Residual complex % in D_2O [a]	Residual complex % in DMEM-d [a]
1	$3.8 \cdot 10^{-1}$	< –2	99	84
2	$2.8 \cdot 10^{-2}$	–0.44	65	27
3	$< 1 \cdot 10^{-4}$	0.55	88 [b]	95 [c]
4	$< 1 \cdot 10^{-4}$	0.70	99 [b]	99 [c]

3. Biological studies

3.1. Cytotoxicity

The antiproliferative activity of ligands and complexes was evaluated on three human cancer cell lines, i.e. A2780 (ovarian) and its cisplatin-resistant derivative A2780cis, and A549 (lung). Additionally, the non-tumorigenic cell lines human HEK 293T (embryonic kidney) and BJ (fibroblast) were considered. The results are compiled in Table 2. Complexes **1** and **2** are inactive in all the investigated cell lines, while **3** and **4** are cytotoxic, although they show modest selectivity towards cancer cells. There is a reasonable correlation between **3** and **4** and their respective ligands, **tpm^{IBU}** and **tpm^{FLU}**, in terms of activity, with the iron fragment slightly increasing the overall cytotoxicity.

Table 2. IC_{50} values (μM) determined for ligands, iron complexes and cisplatin on A2780, A2780cis and HEK 293T cell lines after 72 h exposure. The values represent the mean calculated from three independent experiments ± standard deviation.

	A2780	A2780cis	A549	HEK 293T	BJ
tpm	> 100	> 100	> 100	> 100	> 100
tpm^{OH}	> 100	> 100	> 100	> 100	> 100
tpm^{IBU}	8 ± 2	> 100	20 ± 2	17 ± 5	66 ± 13
tpm^{FLU}	11 ± 4	58 ± 15	44 ± 10	25 ± 14	> 100
1	> 100	> 100	> 100	> 100	> 100
2	> 100	> 100	> 100	95 ± 26	> 100
3	5 ± 1	23 ± 10	15 ± 1	9 ± 2	54 ± 1
4	11 ± 2	36 ± 2	26 ± 3	14 ± 4	94 ± 1
Cisplatin	36 ± 17	97 ± 3	65 ± 10	> 100	86 ± 7

3.2. Enzyme inhibition

The ability of the ligands and complexes to inhibit COX-2 and HNE enzymes was investigated, see Table 3. Complexes **3-4** display an inhibitory capacity towards COX-2 enzymes which is similar to

that of the corresponding tpm-derivatized bioactive ligands, i.e. **tpm^{IBU}** and **tpm^{FLU}**, and superior to that of ibuprofen and flurbiprofen. This feature supports the hypothesis that the antiproliferative activity of the complexes is largely due to the lipophilicity of the bioactive fragments.

Table 3. IC_{50} values (μM) obtained for ligands and complexes in the inhibition of COX-2 and HNE.

Compound	IC_{50} ± SD (μM), COX-2	IC_{50} ± SD (μM), HNE
Tpm	> 500	> 1300
tpm^{OH}	> 500	> 1300
tpm^{IBU}	> 500	----
tpm^{FLU}	377 ± 9	----
1	> 500	712 ± 175
2	> 500	> 1300
3	464 ± 63	397 ± 112
4	371 ± 26	502 ± 90
Ibuprofen	> 3000 [43]	----
Flurbiprofen	719 ± 135 [56]	----

3.3. Nucleic acid interaction studies

To further understand the mechanism of action of the complexes, we investigated their potential interaction with natural double-stranded DNA from calf thymus. Complex **4** was selected for testing as it contains the **tpm^{FLU}** ligand, which contains an extended aromatic moiety that might facilitate intercalation between the DNA base pairs. Since direct spectrophotometric studies were unsuitable for **4** (as it only absorbs in the UV range, overlapping with the DNA signal), a fluorescent indicator displacement (FID) assay was used.[73] In this assay, DNA was saturated with the ethidium intercalator (ethidium bromide, EB), and increasing amounts of **4** were added to the mixture. The results (Figure S28) indicate that complex **4** can compete with EB for binding to DNA. However, at a concentration of **4** more than three times higher than that of EB, only 35% of the fluorescent signal typically associated with the DNA-interacting EB probe was lost. This suggests that while complex **4** can bind DNA, its binding affinity is not very strong. For **3**, the affinity is likely even weaker due to its less

favourable geometry. When **3** and **4** were incubated in H_2O/MeOH (5:3 v/v, 0.70 µM solution) with the nucleotide guanosine 5′-monophosphate (disodium salt, Na_2[GMP]), as a model for DNA binding, mass spectrometry analysis did not reveal the formation of any adducts after 24 h. This supports the hypothesis that **3** and **4** do not readily form covalent bonds with nucleic acids.

3.4. ROS production

As it has been demonstrated that the primary mode of action of iron(II) compounds is related to their capacity to interfere with intracellular redox homeostasis (see Introduction), we also evaluated the ability of representative compounds **2** and **4** to increase the cellular basal production of ROS in human ovarian A2780 cancer cells. As shown in Figure 2, complexes **2** and **4** elicit a similar response pattern and were both modestly effective in increasing the cellular basal hydrogen peroxide production. However, the cellular ROS levels detected after treatment with the two iron(II) tpm compounds were substantially lower compared to the effect induced by antimycin, a well-known inhibitor of mitochondrial Complex III in the respiratory chain.[74] Combined, these results support the hypothesis that compound **4** exerts its cytotoxic effect mainly by inhibiting COX-2 and HNE activity.

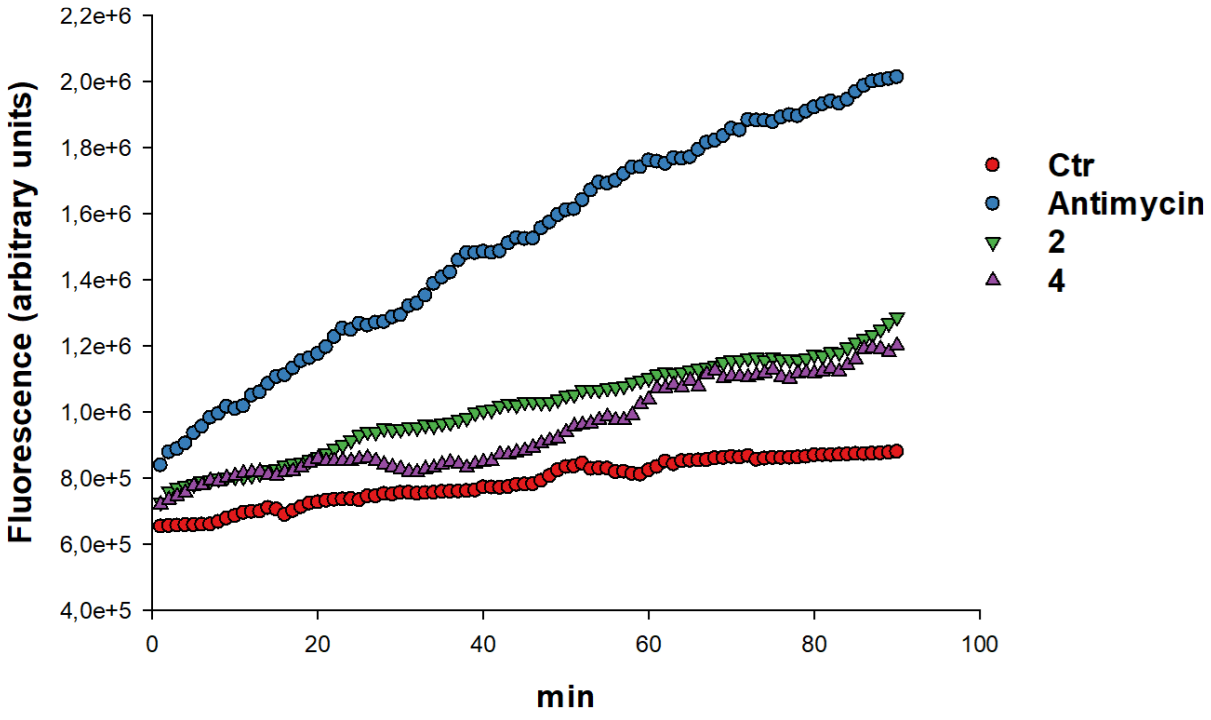

Figure 2. Effect of **2** and **4** on hydrogen peroxide formation in A2780 cancer cells. Cells were pre-incubated in PBS/10 mM glucose medium for 20 min at 37 °C in presence of 10 μM CM–H_2DCFDA and then treated with increasing concentrations of the tested compounds.

4. Concluding remarks

Iron complexes have been extensively investigated as potential novel anticancer drugs with both high efficacy and relevant safety profiles. Here, we present a synthetic strategy aimed at incorporating well-established bioactive groups attached to the trispyrazolylmethane (tpm) skeleton, a robust six-electron donor ligand. These tpm-derivatized ligands were subsequently coordinated to Fe^{2+} in a ferrocene-like, robust sandwich arrangement. The ligands and complexes were assessed for their anticancer potential, and previously reported non-functionalized compounds were also included in this investigation. The obtained results indicate that the cytotoxic activity is observable in compounds with a sufficient degree of lipophilicity, which favours cellular uptake. The active complexes are slightly more cytotoxic than the ligands, suggesting that the observed activity is largely attributable to the bioactive fragment, possibly exerting a specific enzyme inhibitory effect. This observation aligns with the modest stimulation of reactive oxygen species provided by the iron(II) moiety and also lack of binding to nucleotides. Future studies could explore appropriate derivatization of the alcohol group of 2,2,2-tris(pyrazolyl)ethanol, in addition to varying the anion, to develop new iron compounds with an optimal balance of physicochemical and biological properties.

Experimental

1. Materials and methods.

Reactants and solvents were purchased from Alfa Aesar, Merck, Strem or TCI Chemicals, and were of the highest purity available. Tris(1-pyrazolyl)methane (**tpm**) was prepared and purified according to the literature.[75,76] Reactions were conducted under a N_2 atmosphere using standard Schlenk techniques, and all products were stored in air once isolated. Toluene and diethyl ether were dried with a mBraun MB SPS5 solvent purification system, while methanol was distilled over calcium hydride and isopropanol over magnesium. Other solvents were used as received. UV-Vis spectra

(250-800 nm) were recorded on a Ultraspec 2100 Pro spectrophotometer using PMMA cuvettes (1 cm path length). IR spectra of solids were recorded on Agilent Cary630 FTIR spectrometer. UV-Vis and IR spectra were processed with Spectragryph software.[77] NMR spectra were recorded at 298 K on a Jeol JNM-ECZ500R instrument equipped with a Royal HFX Broadband probe. Chemical shifts (expressed in parts per million) are referenced to the residual solvent peaks (^{1}H, ^{13}C) [78] or to external standard (^{19}F to $CFCl_3$). ^{1}H and $^{13}C\{^{1}H\}$ NMR spectra were assigned with the assistance of ^{1}H-^{13}C (*gs*-HSQC and *gs*-HMBC) correlation experiments.[79] Elemental analyses were performed on a Vario MICRO cube instrument (Elementar). ESI-Q/ToF flow injection analysis (FIA) was conducted on solutions of the samples (**1** in octanol, **3** and **4** in methanol) using a 1200 Infinity HPLC coupled to a Jet Stream ESI interface with a Quadrupole-Time of Flight tandem mass spectrometer 6530 Infinity Q-TOF (Agilent Technologies, USA); data was processed with Mass Hunter Qualitative Analysis software.

2. Synthesis and characterization of ligands

Tri(1*H*-pyrazol-1-yl)methanol, tpm^{OH} (Chart 1)

Chart 1. Structure of **tpm^{OH}** (labelling refers to carbon atoms).

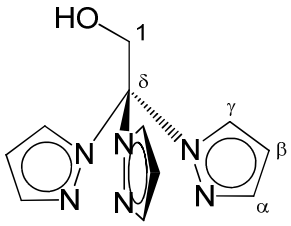

The title compound was prepared using a slightly modified procedure with respect to the literature.[35] A mixture of **tpm** (1.0 g, 4.7 mmol), *para*-formaldehyde (0.36 g, 12 mmol) and potassium *tert*-butoxide, KO^{t}Bu (12 mL of 1 M solution in THF, 12 mmol) in 50 mL of anhydrous THF was stirred at room temperature for 16 h. Water (65 mL) was added and the product was extracted with Et_2O (3 x 30 mL). The organic fractions were dried over Na_2SO_4, filtered, and then the solvent was evaporated under reduced pressure. White crystalline solid, yield 895 mg (78%). Anal. calcd. for $C_{11}H_{12}N_6O$: C,

54.09; H, 4.95; N, 34.41. Found: C, 54.38; H, 5.06; N, 34.28. IR (solid state): $\tilde{\upsilon}/cm^{-1}$ = 3688w-br ($\tilde{\upsilon}_{OH}$), 3206w-br, 1508m, 1425m, 1384m, 1338m, 1321m, 1283m, 1253m, 1239m, 1228m, 1206s, 1110s, 1089m, 1036s, 949m, 915m, 874m, 790m, 758s, 746s. ^{1}H NMR ($CDCl_3$): δ/ppm = 7.71 (d-br, 3H, C$^{\gamma}$H); 7.11 (d, 3H, $^3J_{HH}$ = 2.6 Hz, C$^{\alpha}$H); 6.37 (t, 3H, $^3J_{HH}$ = 2.2 Hz, C$^{\beta}$H); 5.08 (d, 2H, $^3J_{HH}$ = 7.2 Hz, C^{2}H); 4.87 (t, 1H, $^3J_{HH}$ = 7.3 Hz, OH). ^{1}H NMR (CD_2Cl_2): δ/ppm = 7.68 (d-br, 3H, C$^{\gamma}$H); 7.10 (d, 3H, $^3J_{HH}$ = 2.6 Hz, C$^{\alpha}$H); 6.37 (t, 3H, $^3J_{HH}$ = 2.6 Hz, C$^{\beta}$H); 5.02 (d, 2H, $^3J_{HH}$ = 7.3 Hz, C^{2}H); 4.77 (t, 1H, $^3J_{HH}$ = 7.4 Hz, OH). ^{1}H NMR (CD_3OD): δ/ppm = 7.68 (d, 3H, $^3J_{HH}$ = 1.8 Hz, C$^{\gamma}$H); 7.33 (d, 3H, $^3J_{HH}$ = 2.6 Hz, C$^{\alpha}$H); 6.41 (t, 3H, $^3J_{HH}$ = 2.2 Hz, C$^{\beta}$H); 5.05 (s, 2H, C^{2}H). OH not observed. ^{1}H NMR (acetone-d_6): δ/ppm = 7.66 (d, 3H, $^3J_{HH}$ = 1.8 Hz, C$^{\gamma}$H); 7.30 (d, 3H, $^3J_{HH}$ = 2.7 Hz, C$^{\alpha}$H); 6.39 (t, 3H, $^3J_{HH}$ = 2.6 Hz, C$^{\beta}$H); 5.10-5.03 (m, 3H, C^{2}H + OH).

2,2,2-tri(1H-pyrazol-1-yl)ethyl 2-(4-isobutylphenyl)propanoate, tpm^{IBU} (Chart 2)

Chart 2. Structure of **tpm^{IBU}** (labelling refers to carbon atoms).

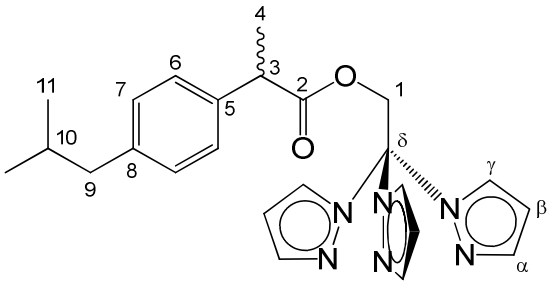

First, 2-(4-Isobutylphenyl)propanoyl chloride was prepared according to the literature,[80] from ibuprofen (racemic mixture, 98 mg, 0.48 mmol) and oxalyl chloride (49 μL, 0.57 mmol). Then, a solution of **tpm^{OH}** (100 mg, 0.82 mmol), freshly prepared 2-(4-isobutylphenyl)propanoyl chloride (105 mg, 0.43 mmol) and anhydrous ethylenediamine (85 μL, 0.61 mmol), in 3 mL of dichloromethane, was stirred at room temperature for 16 h. Afterwards, the volatiles were evaporated under reduced pressure and the crude product was purified by silica chromatography using dichloromethane/diethyl ether mixtures as eluent, with a progressive increase of the relative volume of diethyl ether. Colourless powder, 168 mg (95%). Anal. calcd. for $C_{24}H_{28}N_6O_2$: C, 66.65; H, 6.53;

N, 19.43. Found: C, 66.37; H, 6.64; N, 19.28. IR (solid state): $\tilde{\upsilon}$/cm^{-1} = 3141w, 2961w-br, 1745s (C=O), 1518m, 1421m, 1383m, 1338m, 1319m, 1256m, 1199m, 1152s, 1124m, 1108s, 1091s, 1039s, 1025s, 948m, 916m, 907m, 851m, 790s, 773s, 754s, 736s. ^{1}H NMR ($CDCl_3$): δ/ppm = 7.60 (d, 3H, $^{3}J_{HH}$ = 1.7 Hz, C$^{\gamma}$H); 7.05 (d, 3H, $^{3}J_{HH}$ = 2.6 Hz, C$^{\alpha}$H); 7.04-6.98 (m, 4H, C^{6}H + C^{7}H); 6.26 (dd, 2H, $^{3}J_{HH}$ = 1.8 Hz, $^{3}J_{HH}$ = 2.6 Hz, C$^{\beta}$H); 5.69 (AB system, 1H, $^{2}J_{HH}$ = 12.3 Hz, C^{1}H); 5.61 (AB system, 1H, $^{2}J_{HH}$ = 12.3 Hz, C^{1}H); 3.59 (q, 1H, ^{3}J$_{HH}$ = 7.2 Hz, C^{3}H); 2.44 (d, 2H, ^{3}J$_{HH}$ = 7.2 Hz, C^{9}H); 1.85 (sept, 1H, ^{3}J$_{HH}$ = 6.7 Hz, C^{10}H); 1.40 (d, 3H, ^{3}J$_{HH}$ = 7.2 Hz, C^{4}H); 0.90 (d, 6H, ^{3}J$_{HH}$ = 6.8 Hz, C^{11}H). ^{13}C{^{1}H} NMR ($CDCl_3$): δ/ppm = 172.7 (C^{2}); 141.6 (C$^{\alpha}$); 140.8 (C^{5}); 136.9 (C^{8}); 130.3 (C$^{\gamma}$); 129.4 (C^{6}); 127.4 (C^{7}); 106.8 (C$^{\beta}$); 89.2 (C$^{\delta}$); 66.8 (C^{1}); 45.1 (C^{3}); 45.1 (C^{9}); 30.3 (C^{10}); 22.5 (C^{11}); 17.9 (C^{4}). Crystals of **tpm^{IBU}** suitable for X-ray analysis were obtained by storing the crude reaction mixture at -30 °C.

2,2,2-tri(1H-pyrazol-1-yl)ethyl 2-(2-fluoro-[1,1'-biphenyl]-4-yl)propanoate, tpm^{FLU} (Chart 3)

Chart 3. Structure of **tpm^{FLU}** (labelling refers to carbon atoms).

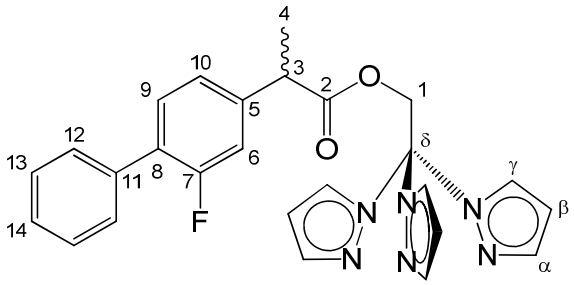

First, 2-(2-fluoro-[1,1'-biphenyl]-4-yl)propanoyl chloride was prepared according to the literature,[81] from flurbiprofen (racemic mixture, 156 mg, 0.64 mmol), oxalyl chloride (300 μL, 3.50 mmol) and a catalytic amount of anhydrous dimethylformamide (3 μL). Afterwards, A solution of **tpm^{OH}** (150 mg, 0.61 mmol), freshly prepared 2-(2-fluoro-[1,1'-biphenyl]-4-yl)propanoyl chloride (racemic mixture, 168 mg, 0.64 mmol) and anhydrous ethylenediamine (130 μL, 0.91 mmol), in 4 mL of anhydrous dichloromethane, was stirred at room temperature for 16 h. The volatiles were evaporated under reduced pressure and the crude product purified by silica chromatography using

dichloromethane/diethyl ether 9:1 v/v mixture as eluent. The resulting colourless oil was kept for several days at -18 °C, and the dried under vacuum to obtain a colourless powder (yield 105 mg, 36 %). Anal. calcd. for $C_{26}H_{23}FN_6O_2$: C, 66.37; H, 4.93; N, 17.86. Found: C, 66.12; H, 4.90; N, 17.72. IR (solid state): $\tilde{\upsilon}/cm^{-1}$ = 3129w-br, 1752s (C=O), 1516m, 1484m, 1419m, 1385m, 1336m, 1318m, 1263m, 1172s, 1109m, 1097m, 1048m, 943m, 927m, 916m, 849m, 838m, 788s, 772, 752s, 730s, 723s, 703s. ^{1}H NMR ($CDCl_3$): δ/ppm = 7.63 (dd, 3H, $^3J_{HH}$ = 1.7 Hz, $^4J_{HH}$ = 0.6 Hz, C$^{\gamma}$H); 7.54-7.43 (m, 4H, C^{12}H+C^{13}H); 7.38 (m, 1H, C^{9}H); 7.32 (t, 1H, $^3J_{HH}$ = 8.0 Hz, C^{14}H); 7.08 (dd, 3H, $^3J_{HH}$ = 2.6 Hz, $^4J_{HH}$ = 0.7 Hz, C$^{\alpha}$H); 6.98 (dd, 2H, $^3J_{HH}$ = 7.9 Hz, $^4J_{HH}$ = 1.8 Hz, C^{10}H); 6.90 (dd, 1H, $^3J_{HF}$ = 11.5 Hz, $^4J_{HH}$ = 1.8 Hz, C^{6}H); 6.28 (dd, 3H, $^3J_{HH}$ = 2.6 Hz, $^4J_{HH}$ = 1.8 Hz, C$^{\beta}$H); 5.76 (AB system, 1H, $^2J_{HH}$ = 12.3 Hz, C^{1}H); 5.64 (AB system, 1H, $^2J_{HH}$ = 12.3 Hz, C^{1}H); 3.68 (q, 1H, $^3J_{HH}$ = 7.2 Hz, C^{3}H); 1.46 (d, 3H, $^3J_{HH}$ = 7.2 Hz, C^{4}H). ^{13}C{^{1}H} NMR ($CDCl_3$): δ/ppm = 172.0 (C^2); 159.7 (d, $^1J_{CF}$ = 247.3 Hz, C^7); 141.8 (C$^{\alpha}$); 140.9 (d, $^3J_{CF}$ = 7.8 Hz, C^5); 135.5 (C^{11}); 130.8 (d, $^3J_{CF}$ = 3.4 Hz, C^9); 130.2 (C$^{\gamma}$); 129.0 (d, $^4J_{CF}$ = 2.9 Hz, C^{12}); 128.7 (C^{13}); 128.1 (d, $^2J_{CF}$ = 13.7 Hz, C^8); 127.9 (C^{14}); 123.8 (d, $^4J_{CF}$ = 3.3 Hz, C^{10}); 115.6 (d, $^2J_{CF}$ = 23.7 Hz, C^6); 106.9 (C$^{\beta}$); 89.2 (C$^{\delta}$); 67.0 (C^1); 45.0 (C^3); 17.75 (C^4). ^{19}F NMR ($CDCl_3$): δ ppm = –117.5 (t, $^3J_{HF}$ = 9.8 Hz).

3. Synthesis and characterization of the iron complexes

$[Fe(\kappa^3\text{-tpm})_2][Cl]_2$, 1 (Chart 4)

Chart 4. Structure of **1** (labelling refers to carbon atoms).

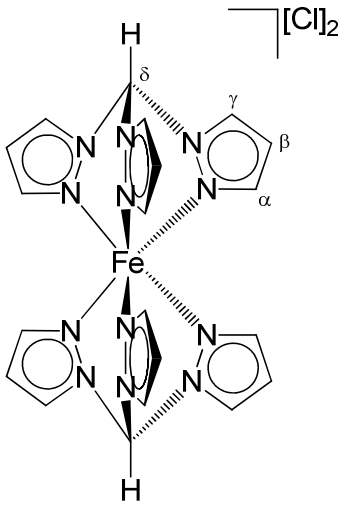

The title compound was prepared using a slightly modified procedure with respect to the literature.[60] A solution of $FeCl_2 \cdot 4H_2O$ (100 mg, 0.50 mmol) and **tpm** (216 mg, 1.00 mmol) in 20 mL of ethanol was stirred at room temperature for 16 h. The product precipitated from the solution as a pink fine powder. The solvent was discarded after centrifugation, and the solid was washed twice with ethanol and then dried under vacuum to afford a pink solid, yield 165 mg (60%). Anal. calcd. for $C_{20}H_{20}Cl_2FeN_{12}$: C, 43.27; H, 3.63; N, 30.27. Found: C, 43.09; H, 3.55; N, 30.36. IR (solid state): $\tilde{\upsilon}/cm^{-1}$ = 3121w, 3112w, 3091w, 1515w, 1439m, 1407m, 1401m, 1284s, 1247m, 1221w, 1088m, 1054m, 982w, 976w, 904w, 899w, 863m, 852m, 785s, 769s, 760s. ^{1}H NMR (D_2O): δ/ppm = 9.12 (s-br, 1H, $C^{\delta}H$); 8.48 (s-br, 3H, CH^{tpm}); 7.78 (s-br, 3H, CH^{tpm}); 7.05 (s-br, 3H, CH^{tpm}). $^{13}C\{^1H\}$ NMR (D_2O): δ/ppm = 158.0, 141.5, 113.3 (CH^{tpm}); 73.5 ($C^{\delta}H$). X-ray quality crystals of $[Fe(\kappa^3\text{-pm})_2][PF_6]_2$, **1'**, were obtained as follows: a sample of **1** was treated with a 4-fold excess of NH_4PF_6 in water; the obtained solid was washed with a small volume of water and redissolved in acetone; crystals finally formed upon slow evaporation of the solvent. HPLC-MS(+): m/z found 519.0998 [**3** – Cl]$^+$, calcd. for $C_{20}H_{20}ClFeN_{12}$ 519.0972. The isotopic pattern fits well the calculated one.

$[Fe(\kappa^3\text{-tpm}^{OH})_2][Cl]_2$, 2 (Chart 2)

Chart 2. Structure of **2** (labelling refers to carbon atoms).

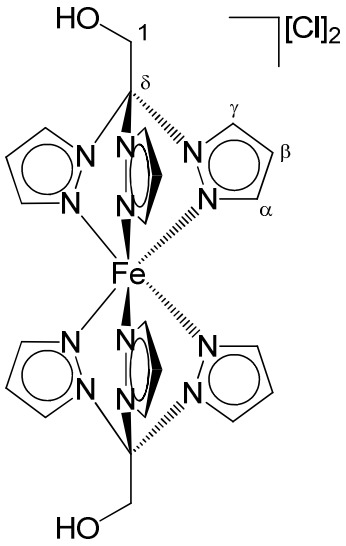

The title compound was prepared using a slightly modified literature procedure.[66] A solution of $FeCl_2 \cdot 4H_2O$ (45 mg, 0.23 mmol) and **tpm^{OH}** (118 mg, 0.48 mmol), in 8 mL of anhydrous methanol, was stirred at room temperature for 16 h. The solution was concentrated under reduced pressure and the product was precipitated upon addition of diethyl ether (ca. 30 mL). The solid residue was filtered, washed with diethyl ether and then dried under vacuum to afford a red solid, yield 103 mg (73%). Anal. calcd. for $C_{22}H_{24}Cl_2FeN_{12}O_2$: C, 42.95; H, 3.93; N, 27.32. Found: C, 43.06; H, 4.03; N, 27.16. IR (solid state): $\tilde{\upsilon}/cm^{-1}$ = 3377w (OH), 3118w, 1620w, 1515w, 1413m, 1395m, 1336m, 1319m, 1225s, 1105m, 1086s, 1067m, 976w, 923w, 868s, 755s, 748s. ^{1}H NMR (CD_3OD): δ/ppm = 8.76 (s-br, 3H, CH^{tpm}); 7.32 (s-br, 3H, CH^{tpm}); 6.62 (s-br, 3H, CH^{tpm}); 5.86 (s-br, 2H, C^{1}H). OH not observed. ^{13}C{^{1}H} NMR (CD_3OD): δ/ppm = 151.1, 137.6, 110.7 (CH^{tpm}); 85.5 (C$^{\delta}$); 61.2 (C^1). ^{1}H NMR (DMSO-d_6): δ/ppm = 7.62 (s-br, 3H, CH^{tpm}); 7.41 (s-br, 3H, CH^{tpm}); 6.36 (s-br, 3H, CH^{tpm}); 5.88 (s-br, 1H, OH); 4.92 (s-br, 2H, C^{1}H). ^{13}C{^{1}H} NMR (DMSO-d_6): δ/ppm = 139.7, 129.9, 105.3 (CH^{tpm}); 88.8 (C$^{\delta}$); 64.3 (C^1).

[Fe(κ^3-tpm^{IBU})$_2$][Cl]$_2$, 3 (Chart 2)

Chart 2. Structure of **3** (labelling refers to carbon atoms).

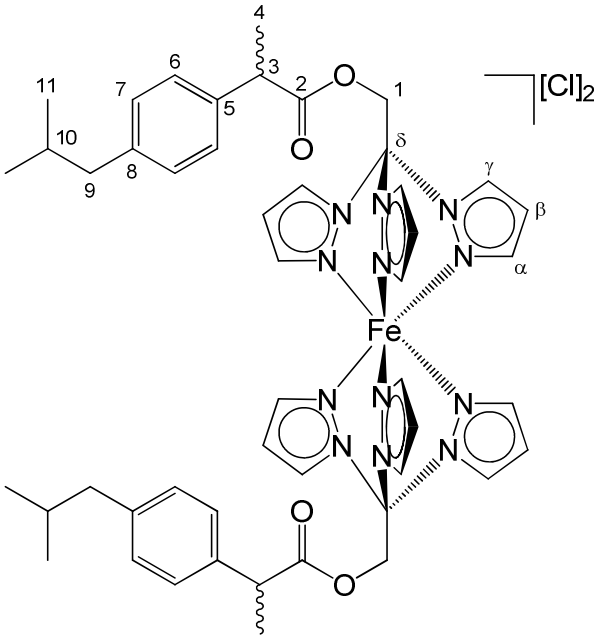

A solution of $FeCl_2 \cdot 4H_2O$ (17 mg, 0.086 mmol) and **tpm^{IBU}** (80 mg, 0.18 mmol), in 3 mL of degassed methanol, was stirred for 16 h at room temperature. The final solution was concentrated under reduced pressure. The precipitation of the product was completed by addition of diethyl ether (20 mL) to the concentrated ethanol solution. The solid was filtered, washed with small volumes of diethyl ether and ethanol, and dried under vacuum to afford a pink solid, yield 65 mg (78%). Anal. calcd. for $C_{48}H_{56}Cl_2FeN_{12}O_4$: C, 58.13; H, 5.69; N, 16.95. Found: C, 57.90; H, 5.52; N, 17.08. IR (solid state): $\tilde{\upsilon}/cm^{-1}$ = 3143w, 3115w, 2955w, 2915w, 2867w, 1754m (C=O), 1512w, 1419m, 1399w, 1336m, 1324m, 1224m, 1193w, 1154m, 1140m, 1109m, 1073m, 975w, 930w, 909w, 844m, 836m, 797w, 761m, 749s, 738s. ^{1}H NMR (CD_3OD): δ/ppm = 7.55 (s-br, 3H, C$^{\gamma}$H); 7.14 (s-br, 3H, C$^{\alpha}$H); 6.96 (AB system, 4H, $^3J_{HH}$ = 7.9 Hz, C^{6}H + C^{7}H); 6.28 (s-br, 3H, C$^{\beta}$H); 5.53 (AB system, 2H, $^2J_{HH}$ = 12.2 Hz, C^{1}H); 3.57 (q, 1H, $^3J_{HH}$ = 7.2 Hz, C^{3}H); 2.39 (d, 2H, $^3J_{HH}$ = 6.8 Hz, C^{4}H); 1.79 (m, 1H, C^{10}H); 1.34 (d, 3H, $^3J_{HH}$ = 6.7 Hz, C^{9}H); 0.80 (d, 6H, $^3J_{HH}$ = 6.2 Hz, C^{11}H). ^{13}C{^{1}H} NMR ($CDCl_3$): δ/ppm = 174.1 (C^2); 142.6 (C$^{\alpha}$); 141.7 (C^5); 138.3 (C^8); 131.8 (C$^{\gamma}$); 130.2 (C^6); 128.4 (C^7); 107.7 (C$^{\beta}$); 90.3 (C$^{\delta}$); 54.9 (C^1); 46.0 (C^9); 45.9 (C^3); 31.3 (C^{10}); 22.6 (C^{11}); 18.3 (C^4). ^{1}H NMR (CD_3OD/D_2O 1:1 v/v): δ/ppm = 7.65 (s-br, 3H, C$^{\gamma}$H); 7.17 (s-br, 3H, C$^{\alpha}$H); 6.98 (AB system, 4H, $^3J_{HH}$ = 7.1 Hz, C^{6}H + C^{7}H); 6.38 (s-br, 3H, C$^{\beta}$H); 5.52 (AB system, 2H, $^2J_{HH}$ = 11.9 Hz, C^{1}H); 3.67 (m, 1H, C^{3}H); 2.41 (d, 2H, $^3J_{HH}$ = 6.7 Hz, C^{4}H); 1.78 (m, 1H, C^{10}H); 1.34 (d, 3H, $^3J_{HH}$ = 6.7 Hz, C^{9}H); 0.85 (d, 6H, $^3J_{HH}$ = 6.2 Hz, C^{11}H). The peak of residual CD_3OD was used as reference. HPLC-MS(+): m/z found 955.3624 [**3** – Cl]$^+$, calcd. for $C_{48}H_{56}ClFeN_{12}O_4$ 955.3585. The isotopic pattern fits well the calculated one.

[Fe(κ^3-tpm^{FLU})$_2$][Cl]$_2$, 4 (Chart 4)

Chart 2. Structure of **4** (labelling refers to carbon atoms).

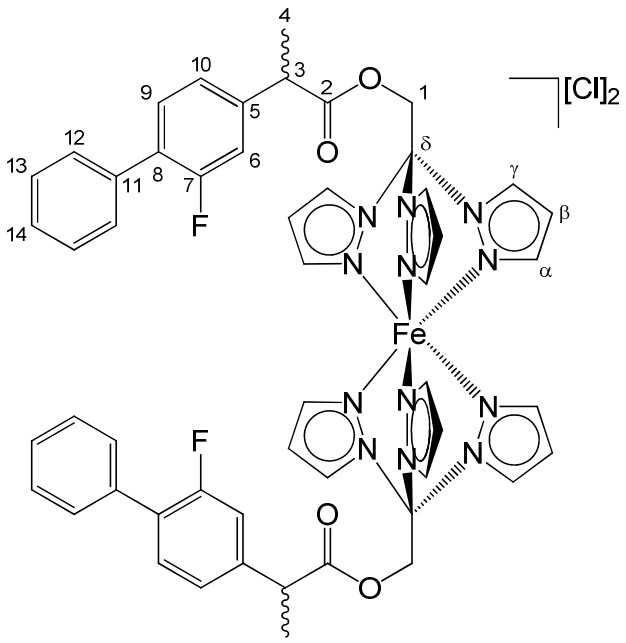

A solution of $FeCl_2 \cdot 4H_2O$ (17 mg, 0.086 mmol) and **tpm^{FLU}** (85 mg, 0.18 mmol), in 3 mL of methanol, was stirred for 16 h at room temperature. The final solution was concentrated under reduced pressure. The precipitation of the product was completed by addition of diethyl ether (20 mL) to the concentrated ethanol solution. The solid was filtered, washed with small volumes of diethyl ether and ethanol, and dried under vacuum to afford a pink solid, yield 50 mg (55%). Anal. calcd. for $C_{52}H_{46}Cl_2F_2FeN_{12}O_4$: C, 58.49; H, 4.34; N, 15.74. Found: C, 58.31; H, 4.45; N, 15.58. IR (solid state): $\tilde{\upsilon}/cm^{-1}$ = 3139w, 2975w, 1750s (C=O), 1623w, 1581w, 1559w, 1516w, 1483w, 1449w, 1417m, 1396m, 1335m, 1323m, 1269w, 1225m, 1199w, 1166m, 1131m, 1107m, 1072m, 1011w, 976w, 936w, 918w, 896w, 870w, 836m, 750s, 698s. ^{1}H NMR (CD_3OD): δ/ppm = 7.49 (s-br, 3H, C$^{\gamma}$H); 7.38 (m, 2H, C^{12}H); 7.31-7.21 (m, 4H, C^{13}H + C^{9}H + C^{14}H); 7.08 (s-br, 3H, C$^{\alpha}$H); 6.89 (d, 1H, $^3J_{HH}$ = 7.7 Hz, C^{10}H,); 6.82 (d, 1H, $^3J_{HF}$ = 11.7 Hz, C^{6}H); 6.23 (s, 3H, C$^{\beta}$H); 5.56 (AB system, 1H, $^2J_{HH}$ = 11.8 Hz, C^{1}H); 5.64 (AB system, 1H, $^2J_{HH}$ = 11.8 Hz, C^{1}H); 3.62 (m, 1H, C^{3}H); 1.30 (d, 3H, C^{4}H, $^3J_{HH}$ = 6.9 Hz). ^{13}C{^{1}H} NMR (CD_3OD): δ/ppm = 173.2 (C^2); 160.5 (d, $^1J_{CF}$ = 247.3 Hz, C^7); 142.5 (C$^{\alpha}$); 142.4 (d, $^3J_{CF}$ = 7.7 Hz, C^{5}H); 136.5 (C^{11}); 131.6 (C$^{\gamma}$); 130.3 (C^9); 129.9 (C^{13}); 128.5 (C^{12}); 128.8 (d, $^2J_{CF}$ = 12.9 Hz, C^8); 128.5 (C^{14}); 124.8 (C^{10}); 116.2 (d, $^2J_{CF}$ = 23.1 Hz, C^6); 107.6 (C$^{\beta}$); 88.9 (C$^{\delta}$); 66.3 (C^1); 44.8 (C^3); 16.7 (C^4). ^{19}F NMR ($CDCl_3$): δ ppm = 121.2 (t, $^3J_{HF}$ = 9.9 Hz). ^{1}H NMR (CD_3OD/D_2O 1:1 v/v): δ/ppm = 7.65 (s-br, 3H, C$^{\gamma}$H); 7.49 (m, 2H, C^{12}H); 7.49-7.32 (m, 4H, C^{13}H + C^{6}H + C^{14}H);

7.21 (s-br, 3H, $C^{\alpha}H$); 6.99 (d, 1H, $C^{10}H$, $^{3}J_{HH}$ = 8.1 Hz); 6.87 (d, 1H, $C^{7}H$, $^{3}J_{HH}$ = 11.2 Hz); 6.39 (s, 3H, $C^{\beta}H$); 5.58 (AB system, 2H, $^{2}J_{HH}$ = 12.3 Hz, $C^{1}H$); 3.81 (m, 1H, $C^{3}H$); 1.42 (d, 3H, $C^{4}H$, $^{3}J_{HH}$ = 7.0 Hz). HPLC-MS(+): m/z found 1031.2852 [**4** – Cl]$^{+}$, calcd. for $C_{52}H_{46}ClF_2FeN_{12}O_4$ 1031.2771. The isotopic pattern fits well the calculated one.

3. Cell culture and cytotoxicity studies

A2780 (RRID: CVCL_0134) and A2780cis (RRID: CVCL_1942) were obtained from the European Collection of Cell Cultures (ECACC, UK) and were cultured in RPMI 1640-Glutamax (Gibco, USA) supplemented with 10% foetal bovine serum (FBS; Sigma-Aldrich, Germany) and Penicillin-Streptomycin (Pen/Strep; Gibco, USA). To sustain cisplatin resistance, the A2780cis cell line was routinely treated with cisplatin (TCI Europe N.V., Belgium) at a concentration of 1 μM. HEK293T (RRID: CVCL_0063) and BJ (RRID:CVCL_3653) were obtained from the American Type Culture Collection (ATCC, USA) and cultured in DMEM-Glutamax (Gibco, USA) supplemented with 10% FBS and Pen/Strep. A549 (RRID:CVCL_0023) was obtained from ATCC and cultured in DMEM-F12 (Gibco, USA) supplemented with 10% FBS and Pen/Strep. All cell lines were maintained in a humidified incubator at 37°C and 5% CO_2.

The tested compounds were dissolved in DMSO at a stock concentration of 10 mM and the concentration course of the compounds was dispensed into 96-well plates (Greiner bio-one, Switzerland) using an Echo acoustic liquid handler (Labcyte Inc., San Jose, CA, USA). Each concentration was dispensed in triplicate, and 10 μM of Gambogic acid (Tocris Bioscience, UK) and an equal amount of DMSO and were dispensed into each plate as a positive and a negative control respectively. The plates were stored at -20°C until use. Before the experiment, the plates were warmed to room temperature and 100 μL of cell suspension (cell concentration $6 \cdot 10^{-4}$ / mL of A2780 and BJ, $1.25 \cdot 10^{-5}$ / mL of A2780cis and HEK293T, $3 \cdot 10^{-4}$ / mL of A549 respectively) was added into each well. After 72 h of incubation the cell viability was evaluated using the MTT assay. MTT(3-(4,5-Dimethylthiazol-2-yl)-2,5-Diphenyltetrazolium Bromide; Invitrogen, USA) reagent was dissolved at

a concentration of 5 mg/mL in phosphate buffered saline (PBS), 10 µL of the solution was added into each well, and the plates were incubated for 3.5 h at 37°C. Then the culture media was carefully aspirated and the formazan crystals were dissolved in DMSO (100 µL per well). The absorbance was measured at 520 nm using Tecan Spark (Tecan, Switzerland) microplate reader and the data was analysed with GraphPad Prism software (version 10.1.0). The reported IC_{50} values are based on the means of three independent experiments.

4. Enzyme activity assays

The enzymatic activity of COX-2 (0.25 U) was fluorimetrically assayed at 576 nm/586 nm at 25 ºC, by measuring the rate of arachidonic acid (ARA) conjugation with COX-2 as a function of time (COX-2 assay kit from Cayman Chemical Company, Ann Arbor, MI, USA). The assay mixture contained 25 µM ADHP, 5 µM hemin, and 37.5 µM ARA in 0.1 M of tris-HCl buffer (pH 8). The inhibitory efficacy was determined by recording the residual activity of COX-2 in the presence of variable concentrations of the analysed compounds (50 - 500 µM). The enzymatic activity of HNE (0.02 UN) was spectrophotometrically assayed at 405 nm at 37 °C for 10 minutes, by measuring the rate of substrate N-succinyl-Ala-Ala-Ala p-nitroanilide (N-suc-ala-ala -ala-pNA) conjugation with HNE. The assay mixture contained 100 µM of N-suc-ala-ala-ala-pNA, 0.1 µM of DMSO, 0.2 M of acetate buffer pH 5.5 in 0.1 M of HEPES buffer pH 7.5. The inhibitory efficacy was determined by recording the residue of HNE activity in the presence of varying concentrations thereof (100 µM - 1300 µM). The IC_{50} value for each compound was obtained using GraphPad Prism 7 software. All the inhibitor assays were performed at least in triplicate, for both analysed enzymes.

5. DNA fluorescent indicator displacement (FID) assay

The FID assay used in this experiment is based on the ethidium fluorophore (ethidium bromide, EB) emitting light when bound to DNA (with maximum excitation at 520 nm and maximum emission at 595 nm), but quenched when free in solution. In the initial part of the experiment (not shown), DNA

was saturated with EB until maximum fluorescence was achieved; then, the tested compound was added to check for any displacement of the probe. CT-DNA (calf thymus DNA), supplied by Merck as a lyophilized sodium salt, was solubilized in ultrapure water. The stock solution underwent sonication procedures for polynucleotides of approximately 500 base pairs.[82] The concentration of the stock solutions (2.33 mM in molarity of base pairs) was determined by UV-vis absorption (NaCac 2.5 mM, pH = 7.0, λ = 260 nm, ε = 13200 M^{-1} cm^{-1}).[83] NaCac is sodium cacodylate (dimethylarsinic acid sodium salt) from Merck (BioXtra, ≥ 98%). Ethidium bromide solid (EB, purity >99%) was obtained from Merck, and the stock solutions were prepared by dissolving known amounts of solid in the buffer. The concentrations were verified spectrophotometrically (λ = 480 nm, ε = 5600 M^{-1} cm^{-1}).[84] The stock solution of the complex **4** (2.06 mM) was obtained by dissolving a known quantity of the solid in DMF (ACS reagent, ≥99.8%, Merck). All aqueous solutions were prepared using ultrapure-grade water by the AriumPro system (Sartorius). Absorption spectra were recorded using a Shimadzu 2450 dual-beam UV-vis spectrophotometer, and the FID assay was performed on a Perkin-Elmer LS55 spectrofluorometer. Both instruments operated at constant temperature using either a Peltier (± 0.1 °C) or a water thermostat (± 0.1 °C).

6. ROS production

The production of ROS was determined in A2780 cells (10^4 per well) grown for 24 h in a 96-well plate in RPMI medium without phenol red (Sigma Chemical Co.). Cells were then washed with PBS and loaded with 10 μM 5-(and-6)-chloromethyl-2′,7′-dichlorodihydrofluorescein diacetate acetyl ester (CM–H_2DCFDA) (Molecular Probes-Invitrogen, Eugene, OR) for 25 min, in the dark. Afterwards, cells were washed with PBS and incubated with increasing concentrations of tested compounds. Fluorescence increase was estimated utilizing the wavelengths of 485 nm (excitation) and 527 nm (emission) in a VICTOR X3 (PerkinElmer, USA) plate reader. Antimycin (3 μM, Sigma Chemical Co), a potent inhibitor of Complex III in the electron transport chain, was used as positive control.

Author contributions

AG, DR and MG: synthesis and characterization of ligands and complexes; SAP, FARM and MLMFSS: enzyme assays; IS, KG and PJD: cytotoxicity tests; SZ: X-ray characterization; TB: biomolecule interactions; CD: evaluation of reactive oxygen species; FM: supervision and writing.

Acknowledgements

We thank the University of Pisa for financial support (Fondi di Ateneo 2022). S. A. P. Pereira acknowledged FCT for her Ph.D. Grant (SFRH/BD/138835/2018). F. A. R. Mota thanks FCT (Fundação para a Ciência e Tecnologia) and ESF (European Social Fund) through POCH (Programa Operacional Capital Humano) for her PhD grant ref. 2022.09611.BD. We thank the Biomolecular Screening Facility (BSF) of the Ecole Polytechnique Fédérale de Lausanne, specifically Julien Bortoli, for technical assistance.

Supporting Information Available

X-ray structure of **1'**; IR and NMR spectra. CCDC reference numbers 2339642 (**1'**) and 2339643 (**tpm^{IBU}**) contain the supplementary crystallographic data for the X-ray studies reported in this work. This data is available free of charge at http://www.ccdc.cam.ac.uk/structures.

The authors declare no competing financial interests.

References

1 E. J. Anthony, E. M. Bolitho, H. E. Bridgewater, O. W. L. Carter, J. M. Donnelly, C. Imberti, E. C. Lant, F. Lermyte, R. J. Needham, M. Palau, P. J. Sadler, H. Shi, F.-X. Wang, W.-Y. Zhang, Z. Zhang, Metallodrugs are unique: opportunities and challenges of discovery and development. Chem. Sci., 2020, 11, 12888–12917.

2 M. Marloye, G. Berger, M. Gelbcke, A survey of the mechanisms of action of anticancer transition metal complexes. Future Med. Chem. 2016, 8, 2263-2286.

3 E. Boros, P. J. Dyson, G. Gasser, Classification of Metal-Based Drugs according to Their Mechanisms of Action. Chem 2020, 6, 41–60.

4 K. L. Haas, K. J. Franz. Application of Metal Coordination Chemistry To Explore and Manipulate Cell Biology. Chem. Rev. 2009, 109, 4921–4960.

5 S. Ghosh, Cisplatin: The first metal based anticancer drug, Bioorg. Chem. 2019, 88, 102925.

6 S. Dilruba, G. V. Kalayda, Platinum-based drugs: past, present and future. Cancer Chemother. Pharmacol. 2016, 77, 1103–1124.

7 R. C. Todd, S. J. Lippard, Inhibition of transcription by platinum antitumor compounds, Metallomics, 2009, 1, 280–291.

8 R. Oun, Y. E. Moussa, N. J. Wheate, The side effects of platinum-based chemotherapy drugs: a review for chemists. Dalton Trans. 2018, 47, 6645–6653.

9 L. Qi, Q. Luo, Y. Zhang, F. Jia, Y. Zhao, F. Wang, Advances in Toxicological Research of the Anticancer Drug Cisplatin, Chem. Res. Toxicol. 2019, 32, 1469−1486.

10 K. Peng, B.-B. Liang, W. Liu, Z.-W. Mao, What blocks more anticancer platinum complexes from experiment to clinic: Major problems and potential strategies from drug design perspectives. Coord. Chem. Rev. 2021, 449, 214210.

11 B. S. Murray, P. J. Dyson, Recent progress in the development of organometallics for the treatment of cancer. Curr. Opinion Chem. Biol. 2020, 56, 28-34.

12 P. Zhang, P. J. Sadler, Advances in the design of organometallic anticancer complexes. J. Organomet. Chem. 2017, 839, 5-14.

13 M. Mora, M. C. Gimeno, R. Visbal, Recent advances in gold–NHC complexes with biological properties. Chem. Soc. Rev. 2019, 48, 447-462.

14 Y. Ching Ong, G. Gasser, Organometallic compounds in drug discovery: Past, present and future, Drug Discovery Today 2020, 37, 117-124.

15 U. Basu, M. Roy, A. R. Chakravarty, Recent advances in the chemistry of iron-based chemotherapeutic agents, Coord. Chem. Rev. 2020, 417, 213339.

16 A. Valente, T. S. Morais, R. G. Teixeira, C. P. Matos, A. I. Tomaz, M. H. Garcia, Ruthenium and iron metallodrugs: new inorganic and organometallic complexes as prospective anticancer agents, Synthetic Inorganic Chemistry, chapter 6, 2021, pp. 223-276, Elsevier ed.

17 G. Gasser, I. Ott, N. Metzler-Nolte, Organometallic Anticancer Compounds, J. Med. Chem. 2011, 54, 3-25.

18 B. Campanella, S. Braccini, G. Bresciani, M. De Franco, V. Gandin, F. Chiellini, A. Pratesi, G. Pampaloni, L. Biancalana, F. Marchetti, The choice of μ-vinyliminium ligand substituents is key to optimize the antiproliferative activity of related diiron complexes, Metallomics 2023, 15, mfac096.

19 S. S. Braga, A. M. S. Silva, A New Age for Iron: Antitumoral Ferrocenes, Organometallics 2013, 32, 5626 − 5639.

20 M. Patra, G. Gasser, The medicinal chemistry of ferrocene and its derivatives. Nat. Chem. Rev. 2017, 1, 10.1038/s41570-017-0066.

21 E. Hwang, H. Sung Jung, Metal–organic complex-based chemodynamic therapy agents for cancer therapy, Chem. Commun., 2020, 56, 8332—8341.

22 A. Vessières, Y. Wang, M. J. McGlinchey, G. Jaouen, Multifaceted chemical behaviour of metallocene (M = Fe, Os) quinone methides. Their contribution to biology, Coord. Chem. Rev. 2021, 430, 213658.

23 T. W. Johnson, R. A. Gallego, M. P. Edwards, Lipophilic Efficiency as an Important Metric in Drug Design, J. Med. Chem. 2018, 61, 6401 – 6420.

24 X. Liu, B. Testa, A. Fahr, Lipophilicity and Its Relationship with Passive Drug Permeation, Pharm Res 2011, 28, 962-977.

25 M. Chen, J. Borlak, W. Tong, high lipophilicity and high daily dose of oral medications are associated with significant risk for drug-induced liver injury, Hepatology 2013, 58, 388-396.

26 M. J. Waring, Lipophilicity in drug discovery, Expert Opin. Drug Discov. 2010, 5, 235-248.

27 Bigmore, H. R.; Lawrence, S. C.; Mountford, P.; Tredget, C. S. Coordination, organometallic and related chemistry of tris(pyrazolyl)methane ligands. Dalton Trans. 2005, 635–651.

28 Reger, D. L. Tris(pyrazolyl)methane ligands: the neutral analogs of tris(pyrazolyl)borate ligands. Comments on Inorganic Chemistry 1999, 21, 1-28.

29 L. M. D. R. S. Martins, C-scorpionate complexes: Ever young catalytic tools, Coord. Chem. Rev. 2019, 396, 89–102.

30 C. Pettinari, R. Pettinari, Metal derivatives of poly(pyrazolyl)alkanes: Tris(pyrazolyl)alkanes and related systems, Coord. Chem. Rev. 2005, 249, 525-543.

31 D. L. Reger, C. A. Little, A. L. Rheingold, R. Sommer, G. J. Long, Synthesis, solid-state structure, magnetic properties and Mössbauer spectral studies of {Fe[HC(3,5-Me2pz)3](H2O)3}(BF4)2, Inorg. Chim. Acta 2001, 316, 65–70.

32 B. Moubaraki, B. A. Leita, G. J. Halder, S. R. Batten, P. Jensen, J. P. Smith, J. D. Cashion, C. J. Kepert, J.-F. Letard, K. S. Murray, Structure, magnetism and photomagnetism of mixed-ligand tris(pyrazolyl)methane iron(II) spin crossover compounds, Dalton Trans., 2007, 4413–4426.

33 B. G. M. Rocha, T. C. O. Mac Leod, M. F. C. Guedes da Silva, K. V. Luzyanin, L. M. D. R. S. Martins, A. J. L. Pombeiro, Ni^{II}, Cu^{II} and Zn^{II} complexes with a sterically hindered scorpionate ligand (TpmsPh)

and catalytic application in the diasteroselective nitroaldol (Henry) reaction, Dalton Trans., 2014, 43 , 15192–15200.

34 C. Pettinari, F. Marchetti, G. Lupidi, L. Quassinti, M. Bramucci, D. Petrelli, L. A. Vitali, M. F. C. Guedes da Silva, L. MDRS Martins, P. Smolenski, A. JL Pombeiro, Synthesis, antimicrobial and antiproliferative activity of novel silver (I) tris (pyrazolyl) methanesulfonate and 1, 3, 5-triaza-7-phosphadamantane complexes, Inorg. Chem. 2011, 50, 11173–11183.

35 D. L. Reger, T. C. Grattan, Synthesis of Modified Tris(pyrazolyl)methane Ligands, Synthesis 2003, No. 3, 350–356.

36 Semeniuc, R. F.; Reger, D. L., Metal Complexes of Multitopic, Third Generation Poly(pyrazolyl)methane Ligands: Multiple Coordination Arrangements, Eur. J. Inorg. Chem.2016, 2253–2271.

37 L. M. D. R. S. Martins, A. J. L. Pombeiro, Tris(pyrazol-1-yl)methane metal complexes for catalytic mild oxidative functionalizations of alkanes, alkenes and ketones, Coord. Chem. Rev. 2014, 265, 74–88.

38 I. A. S. Matias, A. P .C. Ribeiro, E. C. B. A. Alegria, A. J. L. Pombeiro, L. M.D.R.S. Martins, C-scorpionate iron(II) complexes as highly selective catalysts for the hydrocarboxylation of cyclohexane, Inorg. Chim. Acta 2019, 489, 269–274.

39 S. Carlotto, G. Casella, L. Floreano, A. Verdini, A. P.C. Ribeiro, L.M.D.R.S. Martins, M. Casarin, Spin state, electronic structure and bonding on C-scorpionate [$Fe^{(II)}Cl_2$(tpm)] catalyst: An experimental and computational study, Catal. Today 2020, 358, 403–411.

40 L. M. D. R. S. Martins, Catalytic applications of recent metal poly(1H-pyrazol-1-yl)-methane scorpionates, Inorg. Chim. Acta 541, 2022, 121069.

41 A. Notaro, G. Gasser, A. Castonguay, Note of Caution for the Aqueous Behaviour of Metal-Based Drug Candidates, ChemMedChem 2020, 15, 345–348.

42 Cervinka, J.; Gobbo, A.; Biancalana, L.; Markova, L.; Novohradsky, V.; Guelfi, M.; Zacchini, S.; Kasparkova, J.; Brabec, V.; Marchetti, F. Ruthenium(II) Tris-Pyrazolylmethane Complexes Inhibit Cancer Cell Growth by Disrupting Mitochondrial Calcium Homeostasis, J. Med. Chem. 2022, 65, 10567−10587.

43 A. Gobbo, S. A. P. Pereira, L. Biancalana, S. Zacchini, M. L. M. F. S. Saraiva, P. J. Dyson, F. Marchetti, Anticancer Ruthenium(II) Tris(pyrazolyl)methane Complexes with Bioactive Co-ligands, Dalton Trans. 2022, 51, 17050-17063.

44 M. Montani, G. V. Badillo Pazmay, A. Hysi, G. Lupidi, R. Pettinari, V. Gambini, M. Tilio, F. Marchetti, C. Pettinari, S. Ferraro, M. Iezzi, C. Marchini, A. Amici, The water soluble ruthenium(II) organometallic compound [Ru(p-cymene)(bis(3,5 dimethylpyrazol-1-yl)methane)Cl]Cl suppresses triple negative breast cancer growth by inhibiting tumor infiltration of regulatory T cells, Pharmacol. Res. 2016, 107, 282-290.

45 T. R. Steel, F. Walsh, A. Wieczorek-Błauz, M. Hanif, C. G. Hartinger, Monodentately-coordinated bioactive moieties in multimodal half-sandwich organoruthenium anticancer agents, Coord. Chem. Rev. 2021, 439, 213890.

46 S. Movassaghi, E. Leung, M. Hanif, B. YT Lee, H. U Holtkamp, J. KY Tu, T. Söhnel, S. MF Jamieson, C. G. Hartinger, A Bioactive l-Phenylalanine-Derived Arene in Multitargeted Organoruthenium Compounds: Impact on the Antiproliferative Activity and Mode of Action, Inorg. Chem. 2018, 57, 8521–8529.

47 P. Chellan, P. J. Sadler, Enhancing the Activity of Drugs by Conjugation to Organometallic Fragments, Chem. Eur. J. 2020, 26, 8676 – 8688.

48 Q. Cheng, H. Shi, H. Wang, Y. Min, J. Wang, Y. Liu, The ligation of aspirin to cisplatin demonstrates significant synergistic effects on tumor cells, Chem. Commun., 2014, 50, 7427—7430.

49 E. Bortolamiol, F. Visentin, T. Scattolin, Recent Advances in Bioconjugated Transition Metal Complexes for Cancer Therapy, Appl. Sci. 2023, 13, 5561.

50 L. Biancalana, L. K. Batchelor, A. De Palo, S. Zacchini, G. Pampaloni, P. J. Dyson, F. Marchetti, A general strategy to add diversity to ruthenium arene complexes with bioactive organic compounds via a coordinated (4-hydroxyphenyl)diphenylphosphine ligand, Dalton Trans., 2017, 46, 12001–12004

51 C. Sumithaa, M. Ganeshpandian, Half-Sandwich Ruthenium Arene Complexes Bearing Clinically Approved Drugs as Ligands: The Importance of Metal−Drug Synergism in Metallodrug Design, Mol. Pharmaceutics 2023, 20, 1453−1479.

52 K. M. Knights, A. A. Mangoni, J. O. Miners, Defining the COX inhibitor selectivity of NSAIDs: implications for understanding toxicity, Expert Rev. Clin. Pharmacol. 2010, 3, 769-776.

53 FAR Mota, SAP Pereira, ARTS Araujo, MLMFS Saraiva. Evaluation of Ionic Liquids and Ionic Liquids Active Pharmaceutical Ingredients Inhibition in Elastase Enzyme Activity. Molecules 2021, 26, 200.

54 H.-U.-Rehman, T. E. Freitas, R. N. Gomes, A. Colquhoun and D. de Oliveira Silva, Axially-modified paddlewheel diruthenium(II,III)-ibuprofenato metallodrugs and the influence of the structural modification on U87MG and A172 human glioma cell proliferation, apoptosis, mitosis and migration, J. Inorg. Biochem. 2016, 165, 181–191.

55 Z. Li, L. Li, W. Zhao, B. Sun, Z. Liu, M. Liu, J. Han, Z. Wang, D. Li, Q. Wang, Development of a series of flurbiprofen and zaltoprofen platinum(iv) complexes with anti-metastasis competence targeting COX-2, PD-L1 and DNA, J. Inorg. Biochem. 2021, 225, 111596.

56 L. Biancalana, L. K. Batchelor, S. A. P. Pereira, P.-J. Tseng, S. Zacchini, G. Pampaloni, L. M. F. S. Saraiva, P. J. Dyson, F. Marchetti, Bis-conjugation of Bioactive Molecules to Cisplatin-like Complexes through (2,2'-Bipyridine)-4,4'-Dicarboxylic Acid with Optimal Cytotoxicity Profile Provided by the Combination Ethacrynic Acid/Flurbiprofen, Chem. Eur. J. 2020, 26, 17525-17535.

57 L. Biancalana, H. Kostrhunova, L. K. Batchelor, M. Hadiji, I. Degano, G. Pampaloni, S. Zacchini, P. J. Dyson, V. Brabec, F. Marchetti, Hetero-Bis-Conjugation of Bioactive Molecules to Half-Sandwich Ruthenium(II) and Iridium(III) Complexes Provides Synergic Effects in Cancer Cell Cytotoxicity, Inorg. Chem. 2021, 60, 13, 9529–9541.

58 N. Ghosh, R. Chaki, V. Mandal, S. C. Mandal, COX-2 as a target for cancer chemotherapy, 2010, 62, 233–244.

59 S. Misra, K. Sharma, COX-2 Signaling and Cancer: New Players in Old Arena, Curr. Drug Targets 2014, 15, 347-359.

60 L. D. Field, B. A. Messerle, L. P. Soler, T. W. Hambley, P. Turner, Iron(II) complexes containing poly(1-pyrazolyl)methane ligands, J. Organomet. Chem. 2002, 655, 146.

61 A. A. Salaudeen, C. A. Kilner, M. A. Halcrow, Mononuclear and dinuclear iron thiocyanate and selenocyanate complexes of tris-pyrazolylmethane ligands, Polyhedron 2008, 27, 2569-2576.

62 P. A .Anderson, T. Astley, M. A. Hitchman, F. R. Keene, B. Moubaraki, K. S. Murray, B. W. Skelton, E. R. T. Tiekink, H. Toftlund, A. H. White, Structures and spectra of bis-tripodal iron(II) chelates, $[FeL_2]^{2+}$, where L = tris(pyrazol-1-yl)methane, tris(pyridin-2-yl)methane, bis(pyrazol-1-yl)(pyridin-2-yl)methane and tris(pyridin-2-yl)phosphine oxide. Magnetism and spin crossover in the $(pz)_3CH$ case, J. Chem. Soc., Dalton Trans. 2000, 3505.

63 D. L. Reger, C. A. Little, A. L. Rheingold, M. Lam, L. M. Liable-Sands, B. Rhagitan, T. Concolino, A. Mohan, G. J. Long, V. Briois, F. Grandjean, A Synthetic, Structural, Magnetic, and Spectral Study of Several $\{Fe[tris(pyrazolyl)methane]_2\}(BF_4)_2$ Complexes: Observation of an Unusual Spin-State Crossover, Inorg. Chem. 2001, 40, 1508.

64 Neises, B.; Steglich, W. Simple Method for the Esterification of Carboxylic Acids. Angew. Chem., Int. Ed. Engl. 1978, 17, 522 − 524.

65 C. C. McLauchlan, B. L. Smith, R. S. Pippins, B. M. Nelson, 2,2,2-Tris(pyrazol-1-yl)ethanol, Acta Cryst. 2011, E67, o1133–o1134.

66 Silva, T. F. S.; Guedes da Silva, M. F.; Mishra, G. S.; Martins, L. M. D. R. S.; Pombeiro, A. J. L.; Synthesis and structural characterization of iron complexes with 2,2,2-tris(1-pyrazolyl)ethanol ligands: Application in the peroxidative oxidation of cyclohexane under mild conditions, J. Organomet. Chem. 2011, 696, 1310-1318.

67 G. Bresciani, N. Busto, V. Ceccherini, M. Bortoluzzi, G. Pampaloni, B. Garcia, F. Marchetti, Screening the biological properties of transition metal carbamates reveals gold(I) and silver(I) complexes as potent cytotoxic and antimicrobial agents, J. Inorg. Biochem. 2022, 227, 111667.

68 T. Rundlöf, M. Mathiasson, S. Bekiroglu, B. Hakkarainen, T. Bowden, T. Arvidsson, *J. Pharm. Biomed. Anal.* 2010, **52**, 645–651.

69 S. Dasari, P. B. Tchounwou, Cisplatin in cancer therapy: Molecular mechanisms of action. Eur. J. Pharmacol. 2014, 740, 364–378.

70 N. M. Rice, H. M. N. H. Irving and M. A. Leonard, *Pure Appl. Chem*. 1993, **65**, 2373-2396.

71 L. Biancalana, L. K. Batchelor, T. Funaioli, S. Zacchini, M. Bortoluzzi, G. Pampaloni, P. J. Dyson and F. Marchetti, *Inorg. Chem.* 2018, **57**, 6669-6685.

72 a) OECD Guidelines for Testing of Chemicals, in OECD, Paris: 1995; Vol. 107. b) J. C. Dearden, G. M. Bresnen, *Quant. Struct.-Act. Relat*. 1988, **7**, 133-144.

73 S. L. Wicks, A. E. Hargrove, Fluorescent indicator displacement assays to identify and characterize small molecule interactions with RNA, Methods 2019, 167, 3-14.

74 E. C. Slater, The Mechanism Of Action Of The Respiratory Inhibitor, Antimycin, Biochimica et Biophysica Acta 1973, 301, 129-154.

75 D. L. Reger, T. C. Grattan, K. J. Brown, C. A. Little, J. J. S. Lamba, A. L. Rheingold, R.D. Sommer, Syntheses of tris(pyrazolyl)methane ligands and {[tris(pyrazolyl)methane]$Mn(CO)_3$}SO_3CF_3 complexes: comparison of ligand donor properties. J. Organomet. Chem. 2000, 607, 120–128.

76 M. Guelfi, F. Puntoriero, S. Serroni, G. Denti, Dinuclear Tris(1-pyrazolyl)methane Complexes of Ruthenium(II), Eur. J. Inorg. Chem. 2011, 709-720.

77 F. Menges, "Spectragryph - optical spectroscopy software", Version 1.2.5, @ 2016-2017, http://www.effemm2.de/spectragryph.

78 G. R. Fulmer, A. J. M. Miller, N. H. Sherden, H. E. Gottlieb, A. Nudelman, B. M. Stoltz, J. E. Bercaw, K. I. Goldberg, NMR Chemical Shifts of Trace Impurities: Common Laboratory Solvents, Organics, and Gases in Deuterated Solvents Relevant to the Organometallic Chemist. Organometallics, 2010, 29, 2176–2179.

79 W. Willker, D. Leibfritz, R. Kerssebaum, W. Bermel, Gradient selection in inverse heteronuclear correlation spectroscopy. Magn. Reson. Chem., 1993, 31, 287-292.

80 M. Siebert, G. Storch, F. Rominger, O. Trapp, Temperature-Controlled Bidirectional Enantioselectivity in Asymmetric Hydrogenation Reactions Utilizing Stereodynamic Iridium Complexes, Synthesis, 2017, 49, 3485-3494.

81 A. Asghar, M. Yousuf, G. Fareed, R. Nazir, A. Hassan, A. Maalik, T. Noor, N. Iqbal, L. Rasheed, Synthesis, acetylcholinesterase (AChE) and butyrylcholinesterase (BuChE) activities, and molecular docking studies of a novel compound based on combination of fl urbiprofen and isoniazide, RSC Adv., 2020, 10, 19346.

82 C. Bazzicalupi, A. Bencini, A. Bianchi, T. Biver, A. Boggioni, S. Bonacchi, A. Danesi, C. Giorgi, P. Gratteri, A. M. Ingraín, F. Secco, C. Sissi, B. Valtancoli, M. Venturini, DNA binding by a new

metallointercalator that contains a proflavine group bearing a hanging chelating unit, Chem. Eur. J. 2008, 14, 184–196.

83 G. Felsenfeld, S. Z. Hirschman, A neighbor-interaction analysis of the hypochromism and spectra of DNA. J. Mol. Biol. 1965, 13, 407-427.

84 M. J. Waring, Complex formation between ethidium bromide and nucleic acids. J. Mol. Biol., 1965, 13, 269-282.